

Decoupling between particulate carbon, nitrogen and biogenic silica export mediated by cyclonic eddies in the North Pacific Subtropical Gyre

Kuanbo Zhou¹, Claudia R. Benitez-Nelson², Jie Huang³, Peng Xiu⁴, Zhenyu Sun¹, and Minhan Dai¹

¹Xiamen University

²University of South Carolina

³Tsinghua University

⁴South China Sea Institute Of Oceanology

November 26, 2022

Abstract

We identified 38 cyclonic eddies (CEs) using satellite altimetry that traversed Station ALOHA in the North Pacific Subtropical Gyre from 1993 to 2018. We separated CE-induced particle export, measured using free floating sediment traps deployed at 150 m, at the center versus the edge and with time since eddy evolution. The fluxes of particulate carbon, nitrogen and biogenic silica (PC, PN and BSi) varied significantly within and among individual eddies depending on season and age. On annual time scales, there was little to no significant PC (1.1-1.3-fold) or PN (1.1-1.2-fold) CE enhancement relative to non-eddy and non-bloom periods. In contrast, BSi fluxes were elevated by an average of 200 {plus minus} 80% (1.3-2.7-fold). Our results confirm that CEs more efficiently export BSi relative to C, suggesting that these elements, central to marine food webs, differ in their mechanisms of export to depth and may contribute to long term ecological change.

1 Decoupling between particulate carbon, nitrogen and biogenic silica export
2 mediated by cyclonic eddies in the North Pacific Subtropical Gyre

3 Kuanbo Zhou^{a*}, Claudia R. Benitez-Nelson^b, Jie Huang^c, Peng Xiu^d, Zhenyu Sun^a and
4 Minhan Dai^a

5 ^aState Key Lab of Marine Environmental Science& College of Ocean and Earth Sciences,
6 Xiamen University, Xiamen 361102, China

7 ^bSchool of the Earth, Ocean & Environment, University of South Carolina, Columbia,
8 South Carolina, USA

9 ^cMinistry of Education Key Laboratory for Earth System Modeling, and Department of
10 Earth System Science, Tsinghua University, Beijing 100084, China

11 ^dState Key Laboratory of Tropical Oceanography, South China Sea Institute of
12 Oceanology, Guangzhou, China

13 *Corresponding author

14 Kuanbo Zhou

15 State Key Laboratory of Marine Environmental Science, Xiamen University

16 Xiamen 361005, China

17 E-mail: kbzhou@xmu.edu.cn

18

19

20 Submitted to *Geophysical Research Letters*

21

22

23

24

25 **Abstract**

26 We identified 38 cyclonic eddies (CEs) using satellite altimetry that traversed Station
27 ALOHA in the North Pacific Subtropical Gyre from 1993 to 2018. We separated CE-
28 induced particle export, measured using free floating sediment traps deployed at 150 m,
29 at the center versus the edge and with time since eddy evolution. The fluxes of particulate
30 carbon, nitrogen and biogenic silica (PC, PN and BSi) varied significantly within and
31 among individual eddies depending on season and eddy age. On annual time scales, there
32 was little to no significant PC (1.1-1.3-fold) or PN (1.1-1.2-fold) CE enhancement
33 relative to non-eddy and non-bloom periods. In contrast, BSi fluxes were elevated by an
34 average of $200 \pm 80\%$ (1.3-2.7-fold). Our results confirm that CEs more efficiently export
35 BSi relative to C, suggesting that these elements, central to marine food webs, differ in
36 their mechanisms of export to depth and may contribute to long term ecological change.

37

38

39

40

41

42

43

44

45

46

47

48 **1. Introduction**

49 Mesoscale eddies are ubiquitous features throughout the world's oceans that redistribute
50 nutrients from depth to the euphotic zone, thus inducing a cascade of biochemical and
51 ecological responses that facilitate the downward export of sinking particles (Mahadevan,
52 2016; McGillicuddy, 2016; Resplandy et al., 2019). It has been estimated that as much as
53 50% of new production in the global ocean may be due to mesoscale eddy pumping
54 (McGillicuddy, 1998). Field observations, however, suggest that significant differences in
55 the magnitude and composition of eddy-induced particle export occur depending on the
56 mechanism of formation, sampling relative to eddy age, location of sampling within a
57 mesoscale feature, and appropriate non-eddy references (Bidigare et al., 2003; Benitez-
58 Nelson et al., 2007; Buesseler et al., 2008; McGillicuddy et al., 2007; McGillicuddy,
59 2016; Zhou et al., 2020). Therefore, a comprehensive understanding of mesoscale eddy
60 type, the eddy's physical and biogeochemical evolution, and inherent spatial
61 heterogeneity is needed. The ephemeral nature of mesoscale features, however, makes
62 high-resolution field observations difficult. Given this limitation, temporal studies of
63 specific mesoscale eddy types may provide insight into their stochastic variability.

64

65 To provide an initial model construct of baroclinic mesoscale features on particulate
66 carbon (PC), particulate nitrogen (PN) and biogenic silica (BSi) export, the present study
67 focuses on Station ALOHA (A Long-term Oligotrophic Habitat Assessment, 22°45'N,
68 158°W), the site of the Hawaii Ocean Time-series (HOT) program located in the North
69 Pacific Subtropical Gyre (NPSG). This oligotrophic region is characterized by low
70 biological production throughout most of the year (Karl and Church 2014, 2017). During

71 July-August, however, N₂-fixation mediated diatom blooms create a seasonal summer
72 export pulse (SEP) of particulate material that is rapidly transported to depths of 4000 m
73 (Karl et al., 2012; Grabowski et al., 2019). Episodic nutrient inputs may also occur due to
74 mesoscale eddies that regularly pass through the region (Huang et al., 2018) and reflect
75 processes that influence the larger scale biogeochemical state of the NPSG ecosystem
76 (Barone et al., 2019). Studies of wind-induced cyclonic eddies (CEs) in the lee of the
77 Hawaiian Islands confirm that these features may contribute to particulate carbon (PC),
78 particulate nitrogen (PN), and biogenic silica (BSi) export depending on their age
79 (Benitez-Nelson et al., 2007; Bidigare et al., 2003; Maiti et al., 2008). Combined with
80 satellite data, the HOT measurement program provides a unique opportunity to explore a
81 range of CE developmental phases (Barone et al., 2019; Mouriño-Carballido, 2009;
82 Sweeney et al., 2003). Here, we synthesize all the available data associated with
83 mesoscale CEs that have passed in close proximity to Station ALOHA from 1993-2018
84 and systematically assess how their spatial and temporal variability influences the
85 magnitude and composition of suspended and sinking particle fluxes.

86

87 **2. Material and Methods**

88 **2.1 Eddy detection**

89 Both CEs and anticyclonic eddies that traversed Station ALOHA from 1993-2018 were
90 obtained by using the Mesoscale Eddy Trajectory Atlas Product from Archiving,
91 Validation and Interpretation of Satellite Oceanographic data (AVISO, note data are only
92 available from 1993). This product provides the type, location, rotational speed, radius (R)
93 and amplitude of global eddies detected each day from multi-mission delayed-time

94 altimetry datasets (e.g., sea surface height (SSH) and sea level anomaly (SLA)) with
95 $1/4^{\circ} \times 1/4^{\circ}$ spatial resolution ([https://www.aviso.altimetry.fr/en/data/products/value-](https://www.aviso.altimetry.fr/en/data/products/value-added-products/global-mesoscale-eddy-trajectory-product.html)
96 [added-products/global-mesoscale-eddy-trajectory-product.html](https://www.aviso.altimetry.fr/en/data/products/value-added-products/global-mesoscale-eddy-trajectory-product.html)). Here, CEs were
97 identified by where the outermost closed contour line of the SSH field coincided with the
98 maximum geostrophic flow (Huang et al., 2017). We further focused on CEs with
99 lifespan ≥ 4 weeks and amplitude ≥ 3 cm (to take into account altimetry uncertainty
100 data of 2-3 cm). The closest CE center to Station ALOHA and corresponding outermost
101 closed SLA contour were subsequently determined for the time period of each ~3-day
102 sediment trap deployment from 1993-2018 (see Figure S1-S4). We defined Station
103 ALOHA as being within the cyclonic eddy core (EC) if it was located inside the
104 outermost closed SLA contour.

105

106 Numerous studies have shown that mesoscale eddies are heterogeneous, with sheer zones
107 that induce additional hotspots of phytoplankton growth (Mahadevan, 2016). Thus,
108 regions outside of the EC, such as the eddy edge (EE) must also be evaluated to examine
109 mesoscale eddy effects on particle fluxes. The outer perimeter of an eddy-affected area,
110 however, is difficult to define; studies based on satellite data set the EE at twice the R of
111 the eddy feature (Chelton et al., 2011b; Gaube et al., 2014), while *in situ* observations of
112 chlorophyll *a* (Chl *a*) and zooplankton indicate a decorrelation length scale for mesoscale
113 features at Station ALOHA to be 2 - 40 km or $< 1.5R$ (Huntley et al., 2006). Here, we
114 identified water column- and sediment trap-derived PC, PN and BSi flux measurements
115 collected at Station ALOHA as “eddy-influenced” if the distance between Station
116 ALOHA and the closest eddy center (D) was less than $2R$. Of the 230 flux measurements

117 made at Station ALOHA, 95 were considered to be eddy-influenced and all were located
118 within the decorrelation length scale of 1.5R. Thirty-eight CEs were identified and are
119 discussed regarding their role in NPSG biogeochemistry and particle export (Table S1
120 and Figure S1-4).

121

122 To investigate the temporal variation of PC, PN and BSi fluxes within CEs as they aged,
123 each eddy was followed since formation by obtaining a time series of SLA at the EC. The
124 lifespan of a CE is generally comprised of an eddy intensification stage, where SLA
125 begins to decline, a mature stage, where SLA reaches a minimum, and a decay stage,
126 where SLA returns to typical ocean conditions. During an eddy's lifespan, however,
127 some features may merge with other eddies, split, or experience multiple intensification
128 periods due to changes in physical conditions (Huang et al., 2017). For ease of analysis,
129 only CEs that maintained their form were included in our analysis of temporal evolution
130 (N = 22 out of 38). The trajectories of CEs at the time of Station ALOHA passage ($D <$
131 $2R$) are shown in Figure 1. More detailed information regarding specific CE SLA
132 evolution and the SLA at the time of *in situ* measurement are shown in Figure S5.

133

134 **2.2 *In situ* measurements at Station ALOHA**

135 Water column concentrations of suspended and sinking PC, PN and BSi were obtained
136 from the Hawaii Ocean Time-series Data Organization & Graphical System (HOT-
137 DOGS) (<http://hahana.soest.hawaii.edu/hot/hot-dogs/interface.html>), and methods are
138 described in detail at <http://hahana.soest.hawaii.edu/hot/methods/results.html>. Details of
139 the elemental sampling and analysis are provided in the Supplemental Material (SM), S1.

140

141 **3. Results**

142 **3.1 Particulate C, N and BSi export mediated by cyclonic eddies**

143 Physical CE properties, including lifespan, age, radius and trajectories, are presented in
144 Figure 1a and the SM, S2. In 6 instances, two *in situ* sampling records were available (see
145 Table S1). To facilitate discussion, we examined the variability of CE-mediated fluxes
146 and inventories at annual and monthly time scales, and separated features into two time-
147 periods: those during bloom (July-August) and non-bloom periods (September-June).

148

149 Particulate C and N eddy inventories (EC + EE) varied from 193 to 396 mmol C m⁻²
150 (average ± standard deviation = 290 ± 46 mmol C m⁻²) and from 31 to 71 mmol N m⁻²
151 (average = 42 ± 7 mmol N m⁻²), with PC sinking fluxes at 150 m ranging from 1.4 to 4.1
152 mmol C m⁻²d⁻¹ (average = 2.5 ± 0.6 mmol C m⁻²d⁻¹) and 0.15 to 0.54 mmol N m⁻²d⁻¹
153 (average = 0.31 ± 0.09 mmol N m⁻²d⁻¹), a greater than 2-fold difference (Figure 1b-c, e-f).
154 Eddy BSi inventories and fluxes were even more variable (>15-fold), ranging from 0.5 to
155 8.6 mmol Si m⁻² and 0.01 to 0.28 mmol Si m⁻²d⁻¹, respectively (Figure 1d and 1g). The
156 range of PC, PN and BSi inventories and fluxes in the EC versus the EE were the same as
157 those for the combined EC+EE (Table S2). These results indicate that CEs triggered
158 higher variability in BSi fluxes relative to PC and PN.

159

160 The magnitude and range of CE PC, PN and BSi inventories and export fluxes also did
161 not significantly differ from those measured during non-eddy periods over an annual time
162 scale (t-tests, p > 0.05) (Table S2). Rather, the monthly variability of CE PC, PN, and BSi

163 inventories and fluxes followed Station ALOHA climatology: high during summer
164 (especially in July and August) and low during spring and winter (Figure S6). To separate
165 CE-influenced signals from Station ALOHA seasonality, we determined all eddy flux and
166 inventory anomalies using the monthly climatological average (MA) (i.e., Eddy-MA)
167 (Table S2). The lowest flux anomalies were observed in August (bloom period), but the
168 timing of the highest flux anomalies differed depending on the element, PC and PN
169 occurred in April and June and BSi in March and April.

170

171 Given the observed seasonal and spatial variability and the inherent difficulty in defining
172 a non-eddy impacted export flux, all CE-mediated export fluxes and inventories were
173 thus normalized to baseline climatology at Station ALOHA: 1) ≤ 2 months before an
174 eddy's passage (EB), 2) ≤ 2 months after an eddy's passage (EA), 3) the MA non-eddy
175 flux and inventory, excluding July and August, 4) the MA of July and August only, and
176 5) the long term non-eddy influenced average (LA) from 1993 to 2018, excluding July-
177 August. It is noteworthy that not every data CE flux and inventory data point
178 corresponded to an EA/EB reference and data collected in July and August were not used
179 for a baseline comparison. For example, for PC fluxes, there were only 22 EB and 18 EA
180 reference data points.

181

182 When CE mediated (EC + EE) particle fluxes were compared to all reference periods
183 (Figure 2, Table S3), average normalized PN eddy fluxes were not significantly different
184 from 1 (from 1.1 ± 0.3 for (EC + EE)/MA excluding July and August to 1.2 ± 0.5 for (EC
185 + EE)/EB). For PC CE fluxes, normalized averages were similarly close to 1 and ranged

186 from 1.1-1.3. Normalized CE PC and PN inventories also did not differ significantly from
187 1 (Figure 2). In contrast, CE-mediated BSi fluxes were both significantly enhanced when
188 normalized to EB (2.65 ± 1.59 , $p = 0.002$) and EA (2.7 ± 3.11 , $p = 0.038$). While CE
189 mediated BSi fluxes were elevated when normalized to MA, excluding July and August
190 (1.3 ± 0.8), and LA (1.3 ± 0.8), they were not significantly different. The lack of
191 statistical significance was likely due to the large variability in BSi fluxes observed
192 within CEs relative to PC and PN. Normalized eddy BSi inventories varied from $1.02 \pm$
193 0.37 (LA) to 1.42 ± 1.83 (EA), but were not significantly different from 1 ($p > 0.05$)
194 (Figure 2). Interestingly, normalized eddy-mediated PC, PN and BSi fluxes during July
195 and August to MA were all significantly < 1 , i.e., 0.83 ± 0.22 , ($p = 0.02$) for PC, $0.81 \pm$
196 0.22 ($p = 0.002$) for PN, and 0.79 ± 0.68 ($p = 0.005$) for BSi.

197

198 We more closely examined differences in EC and EE fluxes. In the EC only, normalized
199 CE BSi fluxes remained > 1 , ranging from 1.8 to 4.3 relative to 1.1-1.4 for PC and 1.2-
200 1.5 for PN, and was significantly enhanced relative to the EA reference. In the EE region
201 only, normalized CE BSi fluxes (1.1-3.0) were still higher than those of PC (1.1-1.2) and
202 PN (1.1-1.2).

203

204 **3.2 Si/C and Si/N ratios in sinking particles**

205 Ratios of Si/C and Si/N in sinking particles were also calculated to examine the relative
206 enhancement of CE BSi fluxes. The range in Si/C ratios (mol:mol) was 0.006 - 0.14, and
207 for Si/N ratios, 0.04 - 1.38, across all CEs. The highest values of both ratios occurred in
208 August CEs under conditions of rapid diatom growth, while for non-eddy periods, Si/C

209 and Si/N ratios ranged from 0.007 to 0.22 and 0.03 to 1.94, respectively. For CEs that
210 passed by Station ALOHA during non-boom periods, Si/C and Si/N ratios ranged from
211 0.006 - 0.089 and 0.04 - 0.72, respectively. Compared to EA and EB reference periods,
212 CE Si/C and Si/N ratios were significantly elevated by 1.1-2.8-fold and 1.1-3.0-fold,
213 respectively (Table S3 and Figure 2).

214

215 **4. Discussion**

216 **4.1 Seasonal variability**

217 Mesoscale CEs enhance biological production, influence food web structure, and hence
218 particle formation and export by facilitating the injection of nutrient rich deep water into
219 the well-lit surface waters (Benitez-Nelson &McGillicuddy, 2008; McGillicuddy, 2016;
220 Resplandy et al., 2019; Zhou et al., 2020). Understanding the magnitude of CE effects on
221 ocean biogeochemistry is confounded by the inherent spatio-temporal variability of the
222 open ocean and the difficulty in not only identifying mesoscale CE features, but also
223 comparing CE-mediated changes to other, presumably uninfluenced ocean waters.

224 Here, eddy-mediated BSi fluxes during non-bloom seasons were found to be elevated
225 relative to PC and PN fluxes and surrounding ocean waters when compared to all non-
226 eddy reference periods, 2 months before or after eddy passage, the monthly average or
227 the long-term annual average. These results agree with previous studies of wind-
228 generated mesoscale eddies that form in the lee of the Hawaiian Islands (e.g., Benitez-
229 Nelson et al., 2007; Maiti et al., 2008). Benitez-Nelson et al. (2007) hypothesized that PC
230 and PN were preferentially remineralized (PN was even more labile than PC) relative to
231 BSi during sinking due to enhanced grazing by microzooplankton. Multiple studies have

232 also found preferential PC remineralization and lower transfer efficiencies relative to BSi
233 in response to the overlying phytoplankton composition, zooplankton grazing strategy
234 and microbial degradation (Karl et al., 1999; Kim, 2017; Reinfelder and Fisher, 1999;
235 Twining et al., 2014). For example, the cyanobacteria *Prochlorococcus spp.* are
236 numerically abundant photoautotrophs in the NPSG, and are more likely to be degraded
237 relative to other cyanobacterial groups due to their semi-permeable proteinaceous
238 membrane (Partensky et al., 1999). Furthermore, elements such as carbon and nitrogen
239 that are incorporated into the algal cytoplasm, are more likely to be assimilated by
240 zooplankton and recycled to the dissolved phase relative to structural elements, such as
241 silica (Reinfelder & Fisher, 1991; Twining et al., 2014). Our results highlight the
242 biogeochemical decoupling between PC, PN and BSi export in response to mesoscale
243 CE-mediated nutrient injection.

244

245 During the bloom season in July and August, CE-mediated PC, PN and BSi fluxes were
246 all reduced. We hypothesized that CEs negatively moderate the physical (e.g., lower
247 temperature and deeper mixed layer depth) and biogeochemical conditions (e.g., higher
248 nitrate intrusion) (Huang et al., 2018) that are favorable for NPSG diatom-diazotroph
249 associations (White et al., 2007), thus ultimately lowering particle fluxes.

250

251 **4.2 Spatial variability**

252 A fundamental characteristic of mesoscale CEs is that their dynamic physical variability
253 (Siegel et al., 2011) influences the biogeochemical response (Barone et al., 2019;
254 Mahadevan, 2008; Zhou et al., 2013). These spatial differences are further influenced by

255 a CE's temporal evolution (Benitez-Nelson & McGillicuddy, 2008; Huang et al., 2017;
256 Sweeney et al., 2003). To more closely examine spatial variability, CE flux and inventory
257 anomalies were assembled in an ideal CE by normalizing the distance between each CE
258 center and Station ALOHA to the CE radius (Figure 3). All anomaly values for fluxes
259 and inventories showed significant spatial variabilities in both the EC and EE, which
260 indicated complex biogeochemical cycling within these mesoscale features. Grouping
261 anomalies into different sub-regions (Table S3), PC and PN inventories in the EC were
262 characterized by high values in the 0.25R-0.5R region, while their fluxes were elevated in
263 the 0.5R-0.75R region. Such spatial mismatches between PC and PN fluxes and
264 inventories further suggested a combination of lateral transport and temporal delays
265 between elevated water column biomass and PC and PN fluxes (Zhou et al, 2013). For
266 BSi, both inventories and fluxes were spatially coherent with highest fluxes within the
267 0.5R-0.75R region, possibly due to more rapid sinking of BSi ballasted material relative
268 to PC and PN.

269

270 Outside the EC, complex physical dynamics processes often result in the coexistence of
271 upwelling and downwelling hotspots that differentially affect PC and PN and BSi export
272 and their inventories (Klein & Lapreye, 2009). No significant spatial trends were
273 observed at the EE as both low and high PC and PN inventories and fluxes were found
274 (Figure 3 and Table S3). In contrast, most of the BSi flux anomalies were positive at the
275 EE. This suggested that BSi fluxes may be preferentially enhanced at the shear zone of
276 the EE relative to PC and PN, possibly due to diatoms bloom induced by submesoscale
277 upwelling (e.g., Mahadevan et al., 2016). Regardless, these results suggest that there may

278 be biases in studies of mesoscale CEs extrapolated from a single observation within the
279 EC (e.g., Bidigare et al., 2003; Sweeney et al., 2003).

280

281 **4.3 Eddy evolution and particle flux**

282 Given the variability associated with physical dynamics at the EE (Siegel et al., 2011),
283 the remaining discussion is focused on EC-defined PC, PN and BSi fluxes and CE
284 evolution age (Figure 4) for those CEs with typical life cycles. We hypothesize that water
285 within the core of the CE is relatively confined. Results indicate that the PC (and PN)
286 flux anomaly was negatively correlated with eddy age (coefficient of determination, $R^2 =$
287 0.30), with highest PC export occurring during early (3 - 8 wk) maturity (highlighted
288 period in Figure 4). In contrast, the PC inventory appeared to temporally increase, with
289 highest inventories occurring later and in the decay stage (>10 wk) (Figure S7). This
290 suggests that PC (and PN) export rapidly declined after the initial phytoplankton bloom
291 and that accumulation of suspended PC (and PN) continued, perhaps due to a transition in
292 the CE food web (Weeks et al., 1993). In contrast, BSi export was high and relatively
293 constant with eddy evolution (Figure 4c). Our results again highlight that PC, PN and BSi
294 are temporally and spatially decoupled within CEs. Such decoupling between PC and BSi
295 fluxes suggest other pathways of carbon export, e.g., subduction of dissolved organic
296 carbon (see SM S3 and Figure S8) (Omand et al., 2015).

297

298 **5. Conclusions**

299 Mesoscale features have been hypothesized to increase PC export to depth in oligotrophic
300 waters of the world's oceans (e.g., Jenkins, 1988). Our results show that 1.1 to 1.3

301 magnitude enhancement of PC export from CEs, mainly during early maturity as they
302 propagate past Station ALOHA in the NPSG. Rather, these mesoscale features resulted in
303 high, but variable BSi export that was typically associated with the EE, but independent
304 of eddy age. Given the low export efficiency of PC relative to that of BSi (see SM S4 and
305 Figure S9), CEs potentially release CO₂ to the atmosphere while also exporting and
306 sequestering silica into the deep ocean. If CEs account for ~15% of the NPSG (Xiu &
307 Chai, 2020), they may increase BSi export by as much as 30%, but only 15% of PC
308 export across the entire NPSG. This result is consistent with our estimates in South China
309 Sea (Zhou et al., 2020). Thus, CEs not only serve as carbon, nitrogen and silica pumps,
310 but also lead to decoupling of critical nutrients needed for the growth of siliceous
311 phytoplankton.

312

313 **Acknowledgements**

314 We thank the scientists and staff of the Hawaii Ocean Time-series (HOT) Program for
315 generating valuable hydrographic and biogeochemical data. We also acknowledge the
316 captains and crew of the R/V *Kilo Moana* and *Kaimikai-O-Kanaloa* for their support of
317 the HOT Program. Drs. David M. Karl and Benedetto Barone are thanked for the
318 valuable comments during the preparation of this manuscript, and their leadership for the
319 HOT program. We especially thank Mingxian Guo for his help with graphics. This
320 research was supported by grants from the National Science Foundation of China
321 (#41730533 and #41890804) and National Science Foundation (OCE-1756517). The data
322 for physical information of the cyclonic eddies are obtained online from Mesoscale Eddy
323 Trajectory Atlas Product from Archiving, Validation and Interpretation of Satellite

324 Oceanographic data ([https://www.aviso.altimetry.fr/en/data/products/value-added-](https://www.aviso.altimetry.fr/en/data/products/value-added-products/global-mesoscale-eddy-trajectory-product.html)
325 [products/global-mesoscale-eddy-trajectory-product.html](https://www.aviso.altimetry.fr/en/data/products/value-added-products/global-mesoscale-eddy-trajectory-product.html)), and biogeochemical data are
326 available from the Hawaii Ocean Time-series Data Organization & Graphical System
327 (<http://hahana.soest.hawaii.edu/hot/hot-dogs/interface.html>).

328

329 **References**

- 330 Barone, B., Coenen, A.R., Beckett, S.J., McGillicuddy, D.J., Weitz, J.S., & Karl, D.M.
331 (2019). The ecological and biogeochemical state of the North Pacific Subtropical
332 Gyre is linked to sea surface height, *Journal of Marine Research*, 77, Supplement,
333 215-245. doi:10.1357/002224019828474241.
- 334 Benitez-Nelson, C. R., Bidigare, R., Dickey, T.D., Landry, M.R., Leonard, C.L., Brown,
335 S.L., et al. (2007). Mesoscale eddies drive increased silica export in the subtropical
336 Pacific Ocean, *Science*, 316, 1017-1021, doi:10.1126/science.1136221.
- 337 Benitez-Nelson, C.R., & McGillicuddy D. J. (2008). Mesoscale physical-biological-
338 biogeochemical linkages in the open ocean: An introduction to the results of the E-
339 Flux and EDDIES programs. *Deep-Sea Research II*, 55, 1133-1138.
340 doi:10.1016/j.dsr2.2008.03.001
- 341 Bidigare, R. R., Benitez-Nelson, C., Leonard, C. L., Quay, P. D., Parsons, M. L., Foley,
342 D. G. & Seki, M. P. (2003). Influence of a cyclonic eddy on microheterotroph
343 biomass and carbon export in the lee of Hawaii, *Geophysical Research Letters*, 30(6),
344 1318, doi:10.1029/2002GL016393.

345 Buesseler, K. O., Lamborg, C., Cai, P., Escoube, E., Johnson, R., Pike, S., et al. (2008).
346 Particle fluxes associated with mesoscale eddies in the Sargasso Sea, *Deep Sea*
347 *Research II*, 55, 1426-1444, doi:10.1016/j.dsr2.2008.02.007.

348 Chelton, D. B., Gaube, P., Schlax, M. G., Early, J. J., & Samelson, R. M. (2011). The
349 influence of nonlinear mesoscale eddies on near-surface oceanic chlorophyll, *Science*,
350 334, 328-332, doi:10.1126/science.1208897.

351 Falkowski, P. G., Ziemann, D., Kolber, Z., & Bienfang, P. K. (1991). Role of eddy
352 pumping in enhancing primary production in the ocean. *Nature*, 352, 55-58,
353 doi:10.1038/352055a0.

354 Gaube, P., McGillicuddy, D. J., Chelton, D. B., Behrenfeld, M. J. & Strutton, P. G.
355 (2014). Regional variations in the influence of mesoscale eddies on near-surface
356 chlorophyll, *Journal of Geophysical Research: Oceans*, 119, 8195-8220,
357 doi:10.1002/2014JC010111.

358 Grabowski, E., Letelier, R.M., Laws, E.A., & Karl, D.M. (2019). Coupling carbon and
359 energy fluxes in the North Pacific Subtropical Gyre. *Nature Communication*, 10,
360 1895, doi:10.1038/s41467-019-09772-z.

361 Guidi, L., Calil, P.R., Duhamel, S., Björkman, K.M., Doney, S.C., Jackson, G.A. et al.
362 (2012). Does eddy-eddy interaction control surface phytoplankton distribution and
363 carbon export in the North Pacific Subtropical Gyre? *Journal Geophysical Research*,
364 117, G02024, doi:10.1029/2012JG001984.

365 Huang, J., Xu, F., Zhou, K., Xiu, P., & Lin, Y. (2017). Temporal evolution of near-
366 surface chlorophyll over cyclonic eddy lifecycles in the Southeastern Pacific, *Journal*
367 *of Geophysical Research: Oceans*, 122, 6165-6179. doi:10.1002/2017JC012915.

368 Huang, J., & Xu, F.H. (2018). Observational evidence of subsurface chlorophyll response
369 to mesoscale eddies in the North Pacific. *Geophysical Research Letters*, 45, 8462-
370 8470. <https://doi.org/10.1029/2018GL078408>

371 Huntley, M. E., Lopez, M. D. G., Zhou, M. & Landry, M. R. (2006). Seasonal dynamics
372 and ecosystem impact of mesozooplankton at Station ALOHA based on optical
373 plankton counter measurements, *Journal of Geophysical Research:Oceans*, 111,
374 C05S10, doi:10.1029/2005JC002892.

375 Jenkins, W. J. (1988). Nitrate flux into the euphotic zone near Bermuda, *Nature*, 331,
376 521-523, doi:10.1038/331521a0.

377 Karl, D. M., Christian, J. R., Dore, J. E., Hebel, D. V., Letelier, R. M., Tupas, L. M., et al.
378 (1996). Seasonal and interannual variability in primary production and particle flux at
379 Station ALOHA, *Deep-Sea Research II*, 43, 539-568 (1999), doi:10.1016/0967-
380 0645(96)00002-1

381 Karl, D. M., Church, M.J., Dore, J.E., Letelier, R.M., & Mahaffey, C. (2012). Predictable
382 and efficient carbon sequestration in the North Pacific Ocean supported by symbiotic
383 nitrogen fixation, *Proceedings of the National Academy of Sciences of the United*
384 *States of America*, 109, 1842-1849, doi:10.1073/pnas.1120312109.

385 Karl, D. M. & Church, M. J. (2014). Microbial oceanography and the Hawaii Ocean
386 Time-series programme, *Nature Review Microbiology*, 12, 1-15.
387 <https://doi.org/10.1038/nrmicro3333>

388 Karl, D. M., & Church, M. J. (2017). Ecosystem structure and dynamics in the North
389 pacific subtropical gyre: new views of an old ocean. *Ecosystems*, 20, 433-457. doi:
390 10.1007/s10021-017-0117-0.

391 Kim, D. (2017). The reduction in the biomass of cyanobacterial N₂ fixer and the
392 biological pump in the northwestern Pacific Ocean, *Scientific Report*, 7, 41810, doi:
393 10.1038/srep41810.

394 Klein, P. & Lapreye, G. (2009), The oceanic vertical pump induced by mesoscale and
395 submesoscale turbulence, *Annual Review of Marine Science*, 1, 351-375,
396 doi:10.1146/annurev.marine.010908.163704.

397 Mahadevan, A. (2008). Comment on “Eddy/wind interactions stimulate extraordinary
398 mid-ocean plankton blooms”, *Science*, 320, 448, doi: 10.1126/science.1152111.

399 Mahadevan, A. (2016). The impact of submesoscale physics on primary productivity of
400 plankton. *Annual Review of Marine Science*, 8, 17.1-17.24. doi:10.1146/annurev-
401 marine-010814-015912.

402 Maiti, K., Benitez-Nelson, C. R., Rii, Y., & Bidigare, R. (2008). The influence of a
403 mature cyclonic eddy on particle export in the lee of Hawaii, *Deep-Sea Research II*,
404 55, 1445-1460. doi:10.1016/j.dsr2.2008.02.008.

405 McGillicuddy, D. J., Robinson, A. R., Siegel, D. A., Jannasch, H. W., Johnson, R.,
406 Dickey, T. D., et al. (1998), Influence of mesoscale eddies on new production in the
407 Sargasso Sea, *Nature*, 394, 263-266, <https://doi.org/10.1038/28367>.

408 McGillicuddy, D. J., Laurence, A.A, Bates, N.R., Bibby, T., Buesseler, K.O., Carlson,
409 C.A. et al. (2007) Eddy/wind interactions stimulate extraordinary mid-ocean plankton
410 blooms, *Science*, 316, 1021-1026, doi:10.1126/science.1136256.

411 McGillicuddy, D. J. (2016). Mechanisms of physical-biological-biogeochemical
412 interaction at the oceanic mesoscale, *Annual Review of Marine Science*, 8, 121-159.
413 doi:10.1146/annurev-marine-010814-015606.

414 Mouriño-Carballido, B. (2009). Eddy-driven pulses of respiration in the Sargasso Sea,
415 *Deep-Sea Research I*, 56, 1242-1250, doi:10.1016/j.dsr.2009.03.001.

416 Nencioli, F., Kuwahara, V. S., Dickey, T. D., Rii, Y. M., and Bidigare, R. R. (2008).
417 Physical dynamics and biological implications of a mesoscale eddy in the lee of
418 Hawai'i: Cyclone Opal observations during E-Flux III, *Deep Sea Research II*, 55,
419 1252-1274, doi:10.1016/j.dsr2.2008.02.003.

420 Omand, M. M., D'Asaro, E.A., Lee, C.M., Perry, M.J., Briggs, N., Cetinić I., Mahadevan,
421 A. (2015). Eddy-driven subduction exports particulate organic carbon from the
422 spring bloom. *Science*, 348(6231), 222-225 (2015).
423 <http://doi.org/10.1126/science.1260062>

424 Partensky, F., Blanchot, J. & Vaulot, D. (1999). Differential distribution and ecology of
425 *Prochlorococcus* and *Synechococcus* in oceanic waters: a review. In: Charpy L,
426 Larkum A (eds) Marine cyanobacteria, vol. 19. Musee Oceanographique, Monaco, pp
427 457-475.

428 Reinfelder, J.R. & Fisher, N. (1999). The assimilation of elements ingested by marine
429 copepods, *Science*, 251,794-796, doi: 10.1126/science.251.4995.794.

430 Resplandy, L., Lévy, M., & McGillicuddy, D. J. (2019). Effects of eddy-driven
431 subduction on ocean biological carbon pump. *Global Biogeochemical Cycles*, 33,
432 1071–1084. <https://doi.org/10.1029/2018GB006125>.

433 Siegel, D., Peterson, P., McGillicuddy, D., Maritorena, S., & Nelson, N. (2011). Bio-
434 optical footprints created by mesoscale eddies in the Sargasso Sea, *Geophysical*
435 *Research Letters*, 38, L13608, doi:10.1029/2011GL047660.

436 Sweeney, E. N., McGillicuddy, D. J. & Buesseler, K. O. (2003). Biogeochemical impacts
437 due to mesoscale eddy activity in the Sargasso Sea as measured at the Bermuda
438 Atlantic Time-series Study (BATS), *Deep-Sea Research II*, 50, 3017-3039,
439 doi:10.1016/j.dsr2.2003.07.008.

440 Twining, B.S., Nodder, S., King, A.L., Hutchins, D.A., LeClerc, G.R., DeBruyn, J.M. et
441 al. (2014), Differential remineralization of major and trace elements in sinking
442 diatoms, *Limnology and Oceanography*, 59, 689-704, doi:10.4319/lo.2014.59.3.0689.

443 Waite, A. M., Stemann, L., Guidi, L., Calil, P. H. R., Hogg, A. M., Feng, M. P. et al.
444 (2016). The wineglass effect shapes particle export to the deep ocean in mesoscale
445 eddies, *Geophysical Research Letters*, 43, 9791-9800, doi:10.1002/2015GL066463.

446 Weeks, A.R., Fasham, M.J.R., Aiken, J., Harbour, D.S., Read, J.F., & Bella J. (1993). The
447 spatial and temporal development of the spring bloom during the JGOFS north
448 Atlantic bloom experiment, 1989, *Journal of Marine Biology Association of United*
449 *Kingdom*, 73, 253-282, doi:10.1017/S0025315400032847.

450 White, A. E., Spitz, Y. H., & Letelier, R. M. (2007). What factors are driving summer
451 phytoplankton blooms in the North Pacific Subtropical Gyre?, *Journal of Geophysical*
452 *Research*, 112, C12006, doi:10.1029/2007JC004129.

453 Xiu, P., & Chai, F. (2020). Eddies affect subsurface phytoplankton and oxygen
454 distributions in the North Pacific Subtropical Gyre. *Geophysical Research Letters*, 47,
455 e2020GL087037. <https://doi.org/10.1029/2020GL087037>

456 Zhou, K., Dai, M., Kao, S., Wang, L., Xiu, P., Chai, F., et al. (2013). Apparent
457 enhancement of ²³⁴Th-based particle export associated with anticyclonic eddies, *Earth*
458 *Planetary Science Letters*, 381, 198-209, doi:10.1016/j.epsl.2013.07.039.

459 Zhou, K., Dai, M., Xiu, P., Wang, L., Hu, J., & Benitez-Nelson, C. R. (2020). Transient
460 enhancement and decoupling of carbon and opal export in cyclonic eddies. *Journal of*
461 *Geophysical Research: Oceans*, 125, e2020JC016372.
462 <https://doi.org/10.1029/2020JC016372>

463

464

465

466

467

468

469

470

471

472

473

474

475

476

477

478

479

480

481

482

483

484 **Figure Caption:**

485 **Figure 1.** Trajectories of the centers of cyclonic eddies (CEs) passing through Station
486 ALOHA from 1993-2018 (a). The red star shows the location of Station ALOHA (158°W,
487 22°45'N)]. Long-term variation of particulate carbon, PC (b), nitrogen, PN (c) and
488 biogenic silica, BSi, flux (d) at 150 m, and 0-150 m inventories of PC (e), PN (f) and BSi
489 (g) at Station ALOHA from 1993-2018. CE-influenced data are indicated by red (EC)
490 and green (EE < 2R) squares; those affected by anticyclonic eddies are excluded.
491 Average non-eddy PC, PN and BSi inventories and fluxes from 1993-2018 are indicated
492 by the solid green line. Average non-eddy PC and BSi inventories and fluxes with data
493 from July and August excluded, are indicated by the dashed green line.

494 **Figure 2.** Box plot of cyclonic eddy (CE)-mediated particulate carbon, PC (a, e),
495 particulate nitrogen, PN (b, f) and biogenic silica, BSi, (c, g) fluxes and inventories
496 normalized to five different reference periods: non-eddy fluxes at Station ALOHA 2
497 months before (EB) and after (EA) a CE passage, monthly average of non-eddy fluxes
498 (MA) with data from July and August excluded and during July and August, and the
499 long-term non-eddy July-August excluded average (LA) of particle fluxes from 1993-
500 2018. Both sinking particle Si/C (d) and Si/N (h) ratios are also compared with reference
501 periods. The 1:1 black dashed line is also shown.

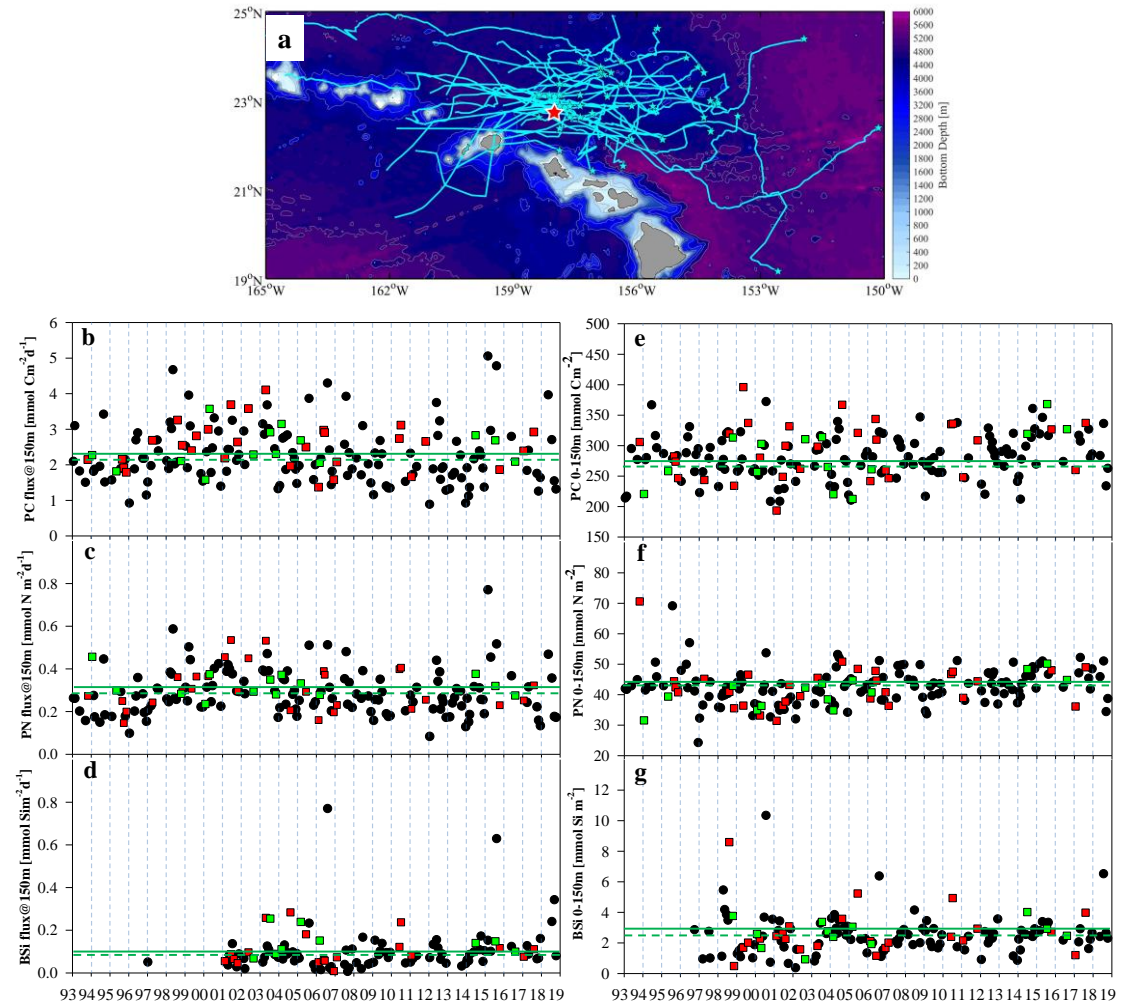
502 **Figure 3.** Spatial variability of cyclonic eddy-mediated particulate carbon, PC, particulate
503 nitrogen, PN and biogenic silica, BSi, fluxes (Eddy - MA) (a, b, c) and inventory
504 anomalies (d, e, f) at Station ALOHA. The distance between each eddy center (based on

505 sea level anomaly, SLA) and Station ALOHA is normalized to $2R$, where R is the
506 average radius of all eddies included in the study. The two circles denote R , $0.25R$, $0.75R$
507 and $1.5R$ distances, respectively.

508 **Figure 4.** Relationship between particulate carbon, PC (a), particulate nitrogen, PN, (b)
509 and biogenic silica, BSi, (c) flux anomalies and cyclonic eddy age within the eddy core
510 ($D \leq R$, Figure 3). Red shading indicates the period when high PC, PN, and BSi flux
511 anomalies were observed; blue and red circles indicate the eddy flux anomalies during
512 July and August, and excluding July and August, respectively. The linear regression
513 equation fitted to all data points and the coefficient of determination, R^2 , are also shown.

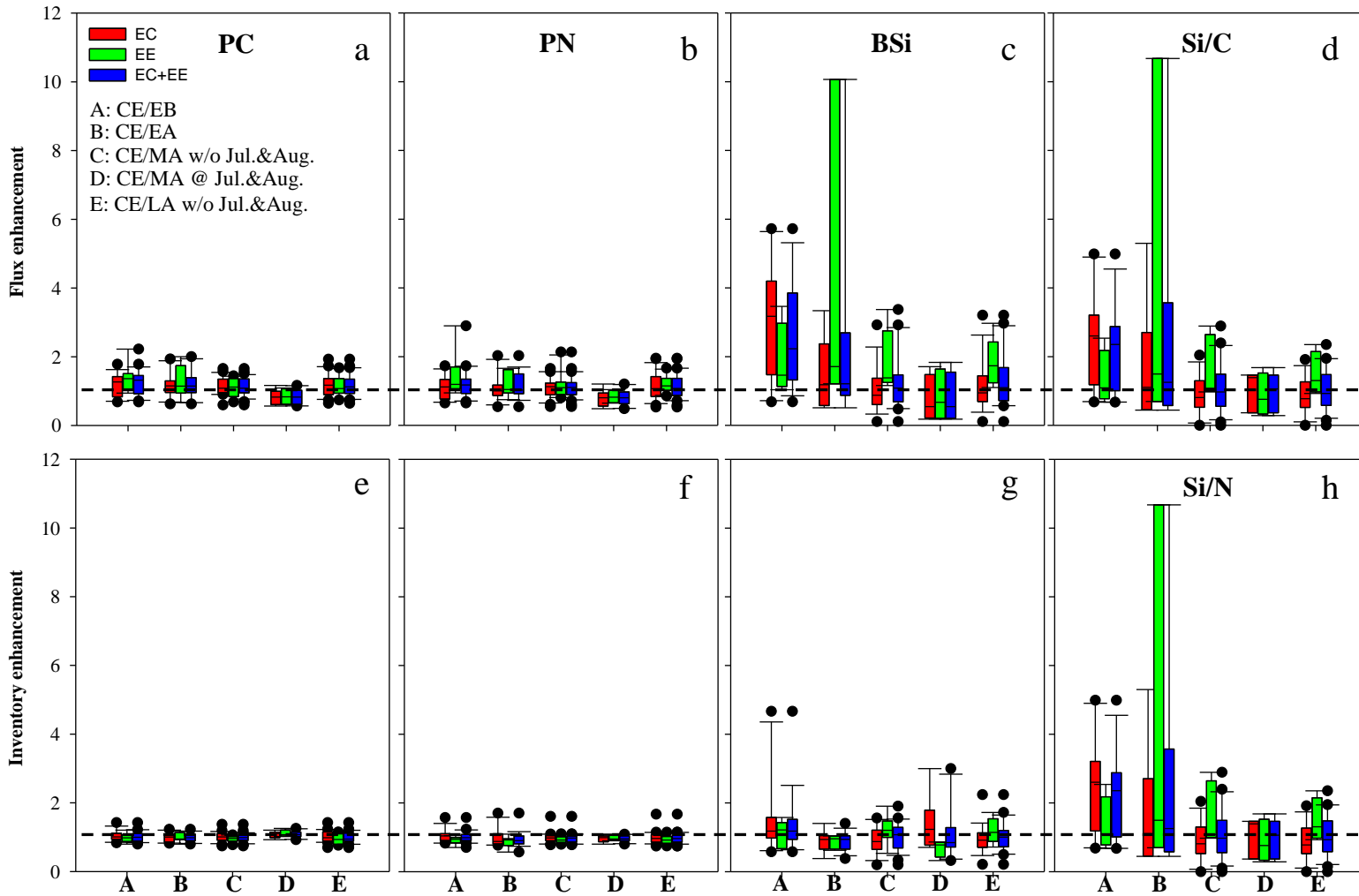
514

515 **Figure 1**

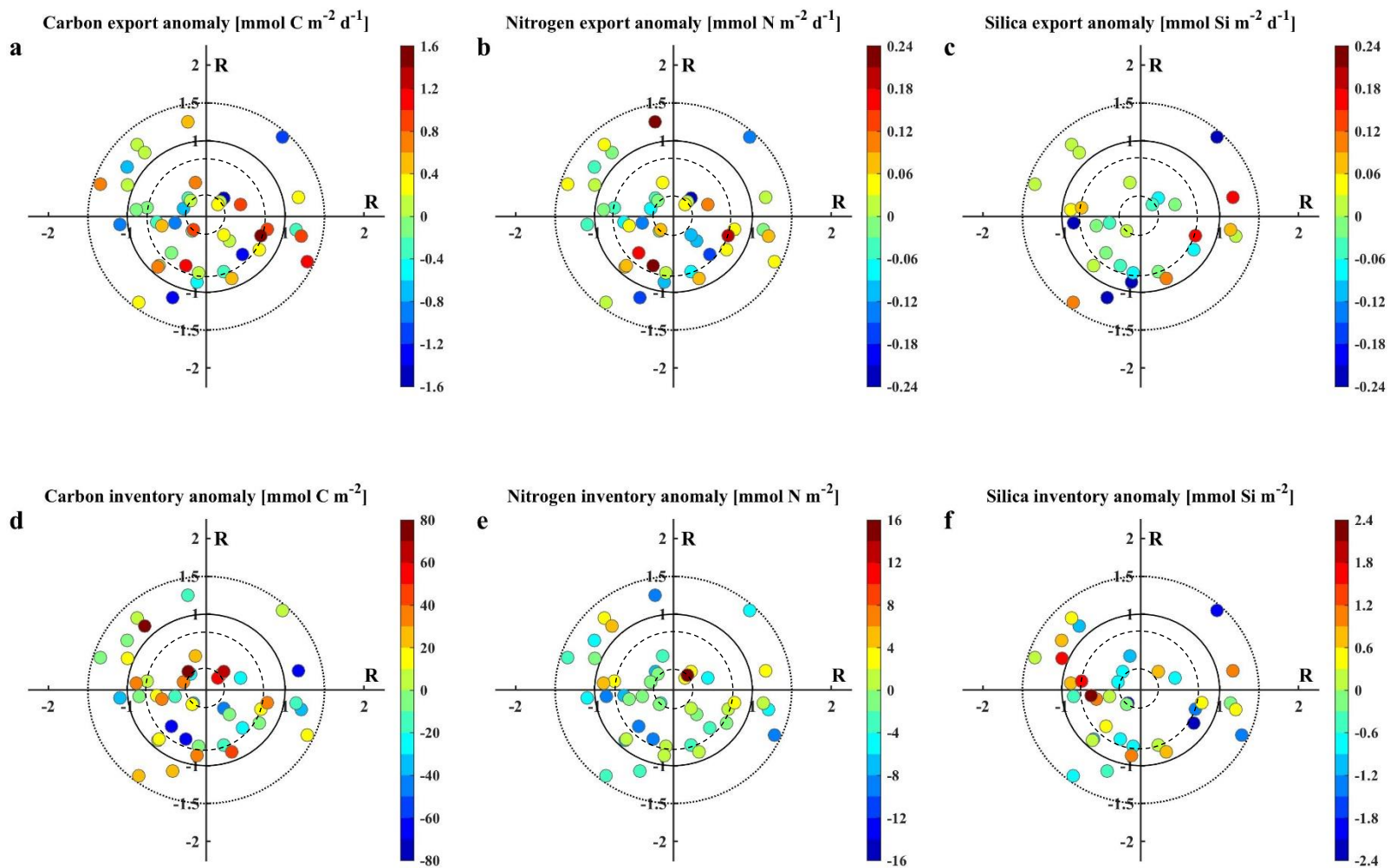


516

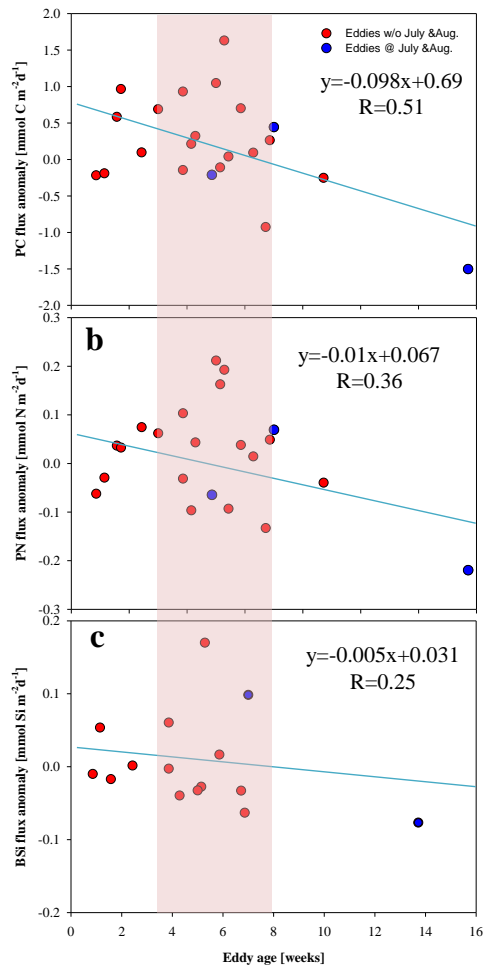
517 **Figure 2**



518



521 **Figure 4**



522

523

524

525